






Multi-method characterization of rare blue quartz-bearing metavolcanic rocks of the Rio dos Remédios Group, Paramirim Aulacogen, NE Brazil

Danielle Cruz da Silva^{1*} , Lauro Montefalco¹ , Gláucia Queiroga² , Glenda Lira Santos¹ , Mahyra Tedeschi³ 

Abstract

The Rio dos Remédios Group comprises a supracrustal sequence that occupies the base of the Espinhaço Supergroup, São Francisco Craton, Brazil. Its basal formation, Novo Horizonte, crops out in the Paramirim region mainly as metavolcanic rocks that represent one of the fewer occurrences of blue quartz phenocrysts in South America. Their mineralogy consists of quartz and K-feldspar phenocrysts, whereas biotite, muscovite, fluorite, allanite, chlorite, sericite, zircon, and opaque phases occur immersed in a quartz-feldspar-rich groundmass. Such heterogeneous composition is also supported by x-ray diffraction and chemical data. Electron probe microanalysis in some samples revealed the presence of two distinct groups of biotite (magmatic and neofomed), in addition to the presence of iron-rich white mica and almost pure orthoclase feldspar. Our data suggest that the studied metavolcanic rocks have maintained their magmatic characteristics, which were progressively overprinted by hydrothermal fluids and ductile-to-brittle deformation. The magmatic mineralogy is akin to strongly peraluminous and alkaline magmas, common in anorogenic settings – a fertile site for the origin of blue quartz-bearing rocks worldwide.

KEYWORDS: blue quartz-bearing rocks petrology; Paramirim Aulacogen; São Francisco Craton

INTRODUCTION

Blue quartz is a rare component of igneous rocks whose origin was formerly discussed in the classical work by Iddings (1904), who suggested that its color results from light scattering due to high concentrations of submicron-sized solid inclusions. So far, there is no consensus regarding the nature of the inclusions in blue quartz (for discussion, see Seifert *et al.* 2011). It has been proposed, however, that the blue color usually reflects the presence of tiny crystals of rutile, ilmenite, magnetite, graphite, biotite, zircon, apatite, tourmaline, or Magnesio-riebeckite (Pantia *et al.* 2019).

Although uncommon in the continental crust, blue quartz crystals are reported in several common lithotypes, including granites, granodiorites, rhyolites, charnockites, and the

metamorphosed products of these rocks, covering approximately 245 occurrences around the world (Pantia *et al.* 2019). Alkaline igneous rocks and their metamorphic correspondents are considered the most fertile sources for the occurrence of this mineral variety (Seifert *et al.* 2011). This association might be explained by unique aspects of the source, including distinctive geochemical character (*e.g.*, metaluminous and peralkaline) and the high temperature of the progenitor magma (Gao *et al.* 2020), which are appropriate conditions favoring the greater inclusion in the blue quartz.

The Paramirim region in NE Brazil is characterized by metavolcanosedimentary sequences, including the Rio dos Remédios Group, which hosts mainly porphyritic metavolcanic rocks composed of centimetric (~2 cm thick) blue quartz phenocrysts, as previously described by Cavalcanti *et al.* (1980). It is suggested that such rocks represent precursor A-type peraluminous magmas, which occupy the base of a thick succession of acid lavas and siliciclastic metasedimentary rocks (*e.g.*, Guimarães *et al.* 2008, Heilbron *et al.* 2017). Among the most famous blue quartz-bearing rocks in South America, such metavolcanic rocks remain poorly investigated, as detailed petrographic/mineralogical studies, as well as the investigation of the possible origin of the blue quartz coloration, have not yet been conducted. As a result, there is a major knowledge gap in the basic characterization of such unique rocks in the continental crust.

This study aimed to present the first petrological-chemical study of the metavolcanic rocks that host blue quartz

¹Departamento de Geologia, Universidade Federal de Pernambuco – Recife (PE), Brasil. E-mails: danielle.cruz@ufpe.br, dani.cs8@live.com, lauro.lisantos@ufpe.br, glenda.lira@ufpe.br

²Departamento de Geologia, Escola de Minas, Universidade Federal de Ouro Preto – Ouro Preto (MG), Brasil. E-mail: glauciaqueiroga@ufop.edu.br

³Programa de Pós-Graduação em Geologia, Universidade Federal de Minas Gerais, Centro de Pesquisas Manoel Teixeira da Costa, Instituto de Geociências, Universidade Federal de Minas Gerais – Belo Horizonte (MG), Brasil. E-mail: mahyratedeschi@gmail.com

*Corresponding author.



phenocrysts of the Rio dos Remédios Group in the Paramirim region, based on detailed petrographic descriptions, x-ray diffraction (XRD), and mineral chemistry. We focus on the major compositional aspects of these rocks, also presenting inferences about their magmatic sources and comparing our occurrences to worldwide examples of (meta)volcanic rocks, which will help further studies about the origin of blue quartz.

GEOLOGICAL SETTING

The study area is located in the morphotectonic domain of the Paramirim Aulacogen, in the northern portion of the São Francisco Craton (Fig. 1). This cratonic block represents a large lithospheric segment composed of Archean terranes that were assembled during subduction-collision events between 2.1 and 2 Ga (Almeida 1977, Barbosa and Sabaté 2003). In terms of reconstructions of Western Gondwana, this craton is limited by Neoproterozoic orogenic domains, including the Araçuaí, Brasília, Rio Preto, Riacho do Pontal, and Sergipano fold belts (Cruz and Alkmim 2007, Rosa 1999, Heilbron *et al.* 2017, Caxito *et al.* 2020). The Paramirim Aulacogen represents an NNW-oriented intracontinental rift system developed from a succession of synclisis aged between 1.70 and 0.65 Ga (Alkmim *et al.* 2007, Danderfer *et al.* 2014, Santana 2016). In a simplified view, it comprises two major lithostratigraphic units:

- the Espinhaço Supergroup (Schobbenhaus 1996);
- the São Francisco Supergroup (Cruz *et al.* 2007).

Both successions were strongly deformed via tectonic inversions that took place during the Neoproterozoic (Guimarães

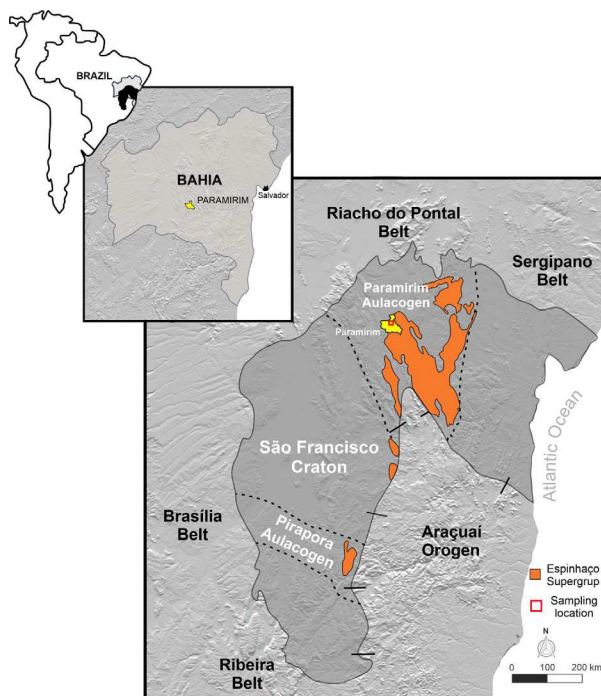
et al. 2005, 2012, Guadagnin and Chemale Jr. 2015, Cruz and Alkmim 2017) and are interpreted as the result of the Brasiliano-Pan African Orogeny (0.8–0.5 Ga; Brito Neves *et al.* 2014), resulting in the development of the intracontinental Paramirim corridor (Alkmim *et al.* 1993, Carlin *et al.* 2018).

The Espinhaço Supergroup is interpreted as a metavolcanosedimentary sequence of predominantly terrigenous and metasedimentary rocks, with acid to intermediate volcanic contributions, mainly at its basal portion (Cruz *et al.* 2007, Medeiros 2013). It comprises the Chapada Diamantina, Paraguaçu, Rio dos Remédios, and Serra da Gameleira sequences (Fig. 2).

The Rio dos Remédios Group encompasses metavolcanic, pyroclastic, and sedimentary rocks, mainly represented by a succession of acid lavas and lacustrine to alluvial sediments, overlaying the sedimentary rocks of the Serra da Gameleira sequence. According to Schobbenhaus and Kaul (1971), this sequence represented the initial stage of rifting, marked by volcanic rocks interleaved with clastic members that encompass the siliciclastic sequence (Guimarães *et al.* 2005, Teixeira 2005, Loureiro *et al.* 2008, Cruz and Alkmim 2017).

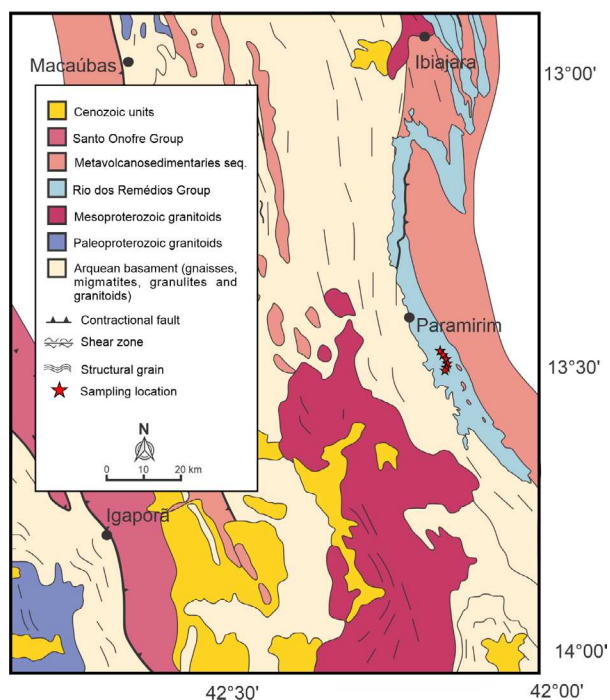
The oldest volcanism of the Rio dos Remédios Group is represented by alkaline A2-type rocks of the Novo Horizonte Formation (Teixeira 2005), crystallized between *ca.* 1752 and 1748 (U/Pb in zircon) (Babinski *et al.* 1994, Schobbenhaus *et al.* 1994), whereas the upper units, Lagoa de Dentro/Ouricuri do Ouro Formation, host the pure sedimentary components of the group.

In the study area, metavolcanic rocks include porphyritic metadacites, metarhyolites, and meta-andesites, usually modified by pervasive deformation and fluid influence of both magmatic and metamorphic origins (Danderfer and Dardenne 2002, Barbosa 2012, Santos *et al.* 2019). The metavolcanic rocks crop



Source: modified from Alkmim *et al.* (2007).

Figure 1. Shuttle Radar Topography Mission (SRTM) map of the São Francisco Craton showing the bordering Neoproterozoic Brasiliano belts, the morphotectonic domain of the Paramirim Aulacogen, the Proterozoic cover sequence (below 1.8 Ga) of the Espinhaço Supergroup, and the sampling location.



Source: modified from Arcanjo *et al.* (1999).

Figure 2. Geological map of the Espinhaço Supergroup in the southeast of Bahia region highlighting the Rio dos Remédios Group and the sampling location.

out as slightly to moderately deformed blocks and boulders of dominant grayish colorations with mesoscopic porphyritic texture, mostly marked by feldspar and blue quartz phenocrysts.

METHODOLOGY

Sample selection

Ten thin sections were selected for petrographic analysis using an Olympus BX51 microscope with an Olympus DP26 camera, at the Gemology Lab of the Universidade Federal de Pernambuco (UFPE), Brazil. Four representative polished thin sections (P4, P5, P6, and P7) were chosen for detailed analysis with XRD, scanning electron microscopy (SEM), and electron microprobe.

X-ray diffraction

The XRD measurements were taken at the Laboratório de Tecnologia Mineral, UFPE, Brazil. The analyses of four samples were performed on a Bruker D2 PHASER using Cu-K α radiation equipped with a Bruker-AXS-Lynxeye detector. The voltage, radiation, and current of the generator were set at 30 kV, 1.54060 Å, and 10 mA ($p = 300$ W), respectively. The diffraction pattern was recorded for 2θ from 4° to 80° with a step scan of 0.02019° in a constant rotation of 10 rpm, counting for 1.5 s at every step. The results were indexed using the app DIFFRAC.EVA with the database COD (REV212673 2018.12.20).

Scanning electron microscopy analysis

The SEM analysis was carried out at the Laboratório de Micropaleontologia Aplicada (LMA), UFPE, Brazil. The four thin sections were selected for image acquisition and qualitative analysis, using a Phenom XL with a backscattered electron detector. The tension, radiation, and current of the generator were set at 15 kV.

Electron probe micro-analyses

The four selected polished thin sections were analyzed using a JEOL JXA-8230 superprobe in the Microscopy and Microanalysis Laboratory at the Universidade Federal de Ouro Preto (UFOP), Brazil. Analyses were conducted at an acceleration voltage of 15 kV, a current of 20 nA, and spot sizes of 5–10 μ m. The analyzed elements and instrumentation standards were as follows: Si (quartz), Na (anorthoclase), K (microcline), Mn (MnO₂), Mg (olivine), Ca (fluorapatite), P (fluorapatite), Al (corundum), Fe (metallic Fe), F (CaF₂), Cl (scapolite), Ba (BaSO₄), Cr (chromite), Sr (strontianite), Ti (rutile), and Zn (gahnite). Counting times on peak and background were 10 and 5 s, respectively, for all elements. ZAF (atomic number, absorption, fluorescence) was the applied common matrix correction.

RESULTS

Field aspects

The studied metavolcanic rocks crop out as highly deformed large blocks and boulders (~2 m long) with common spheroidal

exfoliation along foliation planes that follow the NNE-SSW regional trend typical of the Norte Horizonte sequence (Figs. 3A and 3B). They exhibit a grayish to dark gray color and shades of reddish and greenish yellow when weathered. The rocks are holocrystalline and often porphyritic with phenocrysts of reddish feldspar and opalescent blue quartz phenocrysts (Fig. 3C).

Unlike deformed granitoids, quartz phenocrysts in volcanic rocks maintain their primary volcanic characteristics in intense ductile deformation (Etheridge and Vernon 1981, Williams and Burr 1994), whereas K-feldspar phenocrysts may also be preserved in varying degrees of deformation. Thus, a classical phenocryst classification was used in this work since they represent relic crystals of the deformed volcanic rocks (Vernon 1990).

Quartz phenocrysts exhibit subhedral to anhedral shapes, also occurring as hexagonal bipyramids, ranging from 0.03 to 0.50 cm in diameter. They normally occur surrounded or embayed by the rock matrix. Crystals are mainly milky blue, often eventually exhibiting dark blue rims. The feldspar phenocrysts occur as 4-mm- to 15-cm-long subhedral to euhedral crystals, exhibiting tabular habits. A slightly developed flow orientation is marked by the alignment of elongated eye-shaped crystals. Contrastingly to the quartz crystals, K-feldspar forms clusters of parallel crystals, mostly associated with widespread mineral aggregates (Fig. 3D).

The dominant rock groundmass is grayish to locally light brown, being largely composed of fine-grained quartz + feldspar aggregates, as well as clusters of biotite, chlorite, and sericite lamellae. All studied rocks are widely fractured, including fine-grained mineral clusters that filled the fracture planes, but the mylonitization effect has not been identified.

Mineralogy, petrography, and x-ray measurements

In thin sections, the studied metavolcanic rocks show a dominant grayish color and microstructure that resembles the

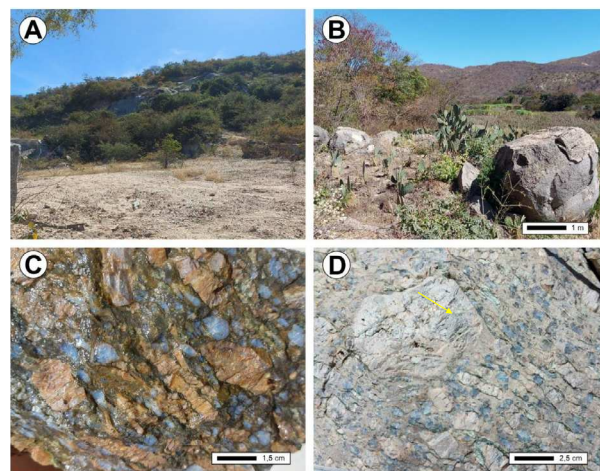


Figure 3. Field and mesoscopic aspects of the Rio dos Remédios metarhyolites. Rocks from the Rio dos Remédios Group are exposed as (A) rhyolitic layers and (B) massive blocks. (C) Porphyritic microstructure highlighting blue quartz and K-feldspar phenocrysts in a deformed volcanic sample. (D) Features of the felsitic groundmass and characteristics of the K-feldspar phenocrysts as clusters of parallel crystals (yellow arrow).

original porphyritic to phaneritic igneous texture. They exhibit well-formed quartz and feldspar phenocrysts, which are surrounded by a thin leucocratic groundmass.

Quartz and K-feldspar are the dominant phases, forming most of the rock phenocrysts with subhedral to anhedral crystalline habits, and accounting for 30% of the rock mode. The very fine-grained matrix is composed of quartz, K-feldspar, and smaller amounts of biotite, zircon, white mica, fluorite, and carbonate. In addition, the main opaque minerals are magnetite, ilmenite, and unidentified iron oxide thin films. The deformation record is well presented on quartz-feldspar-rich groundmass, which is highly affected by deep-seated tectonic processes. In addition to δ and σ porphyroclasts, the groundmass exhibits several deformation markers, including submillimeter-sized quartz-feldspar clots, with rounded shapes and diffuse contacts within thin and strongly recrystallized areas.

Quartz occurs as part of the groundmass and as anhedral porphyroclasts. Their diameter varies from 1 to 5 mm, but larger crystals might be locally observed. Quartz porphyroclasts exhibit rounded to subrounded shapes, also including engulfment textures, which are typical of (meta)volcanic rocks with high silica content (e.g., Silva *et al.* 2016). Magmatic corrosion is widespread, whereas undulose extinction and subgrain rotation are the main markers of the imposed regional deformation (Figs. 4A and 4B). Associated with the edges of the porphyroclasts are crystals formed by subgrain rotation recrystallization, with the same characteristics. Several fractures and microcracks are present and might be filled by epidote, chlorite, carbonate, muscovite, sericite, and micro-crystallized quartz veins.

Similar to the quartz, K-feldspar occurs as subhedral to anhedral megacrystals, presenting up to 0.8 mm in length, and as scattered small crystals in the rock matrix. The crystals are commonly aligned with the primary magmatic flow structures in volcanic rocks and might exhibit well-developed Carlsbad twinning, as well as granophyric and perthite textures (Fig. 4C).

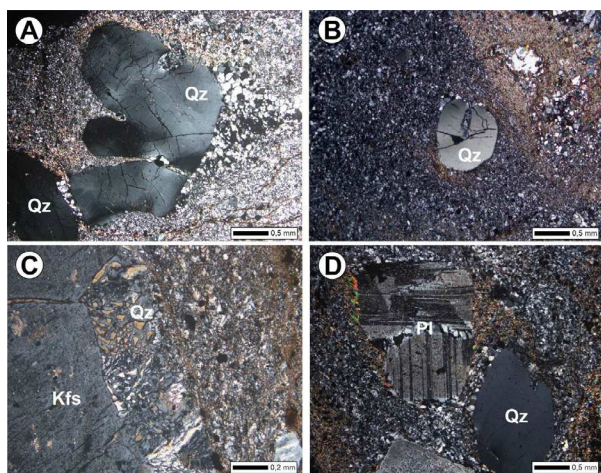


Figure 4. Photomicrographs with cross polarized light from representative samples of the Rio dos Remédios Group metarhyolites. (A) Quartz (Qz) phenocrysts showing rounded to subrounded shapes, undulose extinction, and fractures (B) also displaying engulfment textures. (C) K-feldspar (Kfs) phenocryst exhibiting granophyric texture and (D) plagioclase (Pl) crystal with well-developed albite twinning.

Plagioclase is almost absent in all studied samples, occurring as anhedral to well-formed prismatic crystals. In addition, albite law twinning (Fig. 4C) might be present but is not common. Both feldspar specimens are strongly affected by later alteration (*i.e.*, sericitization and saussuritization) that might reach up to 60% of the crystals. In all samples, this process may be associated with the formation of secondary phases, including carbonate, sericite, and indistinct iron oxides.

Biotite is subhedral to anhedral, light brown to dark brown, and partially chloritized. The crystals form bent-flake lamellae aggregates on the edges of the major crystals, also occurring as inclusions in K-feldspar. It also occurs in contact with muscovite-bearing veins, also containing fluorite, sericite, and variable Fe-Ti oxides (Figs. 5A and 5B). Colorless fluorite is disseminated in the matrix as subhedral crystals, typically 0.1 mm long, and occurs on the edge of micro-crystallized quartz veins within the K-feldspar crystals.

Muscovite occurs as very thin lamellae forming oriented veins along the matrix or surrounding the quartz and feldspar grains, also strongly oriented by the rock metamorphic foliation (Fig. 5C). Zircon, when present, exhibits prismatic and subhedral habits, ranging in size from 0.01 to 0.04 mm, mostly as inclusions in the quartz crystals as well as forming halos on biotite lamellae.

Allanite is present as euhedral to subhedral dark brown crystals. It usually occurs dispersed in the matrix but may form isolated crystals on the edge of phenocrysts (Fig. 5D). Titanite and rutile subhedral crystals are not common but might occur in magnetite- and ilmenite-bearing samples. They usually attain 0.8 mm in length, showing subhedral to euhedral habits, also occurring as tiny inclusions on the phenocrysts.

In most samples, zircon, fluorite, carbonate, magnetite, and ilmenite range in size from 0.02 to 1 mm, occurring as disseminated tiny crystals within the rock groundmass as well as

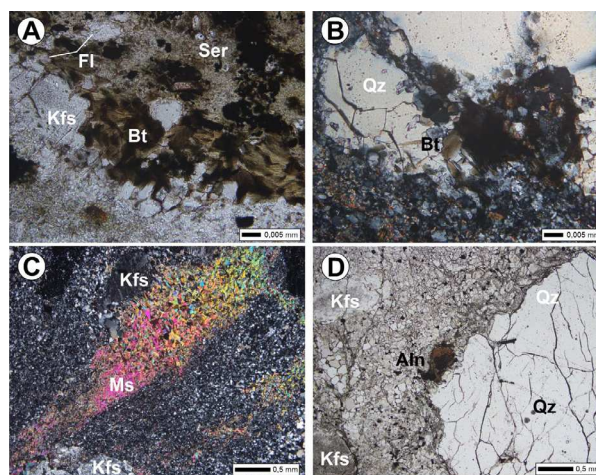


Figure 5. (A, B, C) Representative plane polarized light microphotographs and (D) scanning electron microscopy images. (A) and (B) Characteristics of the biotite (Bt) crystals, strongly chloritized, forming aggregates on the edge of the phenocrysts, usually associated with sericite (Ser), K-feldspar (Kfs), and fluorite (Fl). (C) Oriented veins of muscovite (Ms) as part of the groundmass and (D) overview of the allanite crystals associated with the Fe-Ti opaque components.

inclusions in quartz and K-feldspar in a lesser extent (Fig. 6). Even though there are several inclusions in quartz, their size is not compatible with the size described for Rayleigh scattering in minerals, ranging between 55 and 27 nm (Dörfler 2002). Further studies, using transmission electron microscopy, are necessary to be able to identify and analyze the causes of the blue coloration.

Whole-rock XRD analyses were performed to enhance the mineralogical control of the studied samples of rock blue quartz-bearing metarhyolites. The obtained results are in accordance with the mineralogy described in the petrographic analysis (Fig. 7). The presented diffractograms were indexed according to Wright and Stewart (1968), in which quartz, biotite, albite, microcline, and oligoclase mineral phases were the main rock components. Furthermore, there is a predominance of microcline peaks (M) and, to a lesser extent, albite peaks

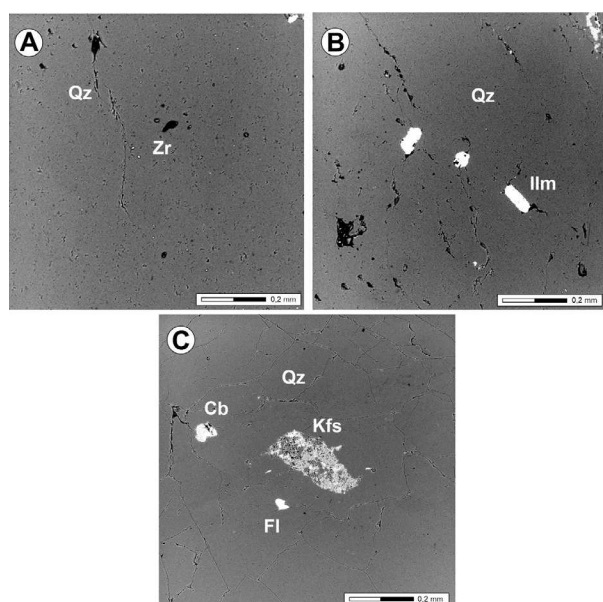


Figure 6. Scanning electron microscopy images of inclusions present in quartz. (A) Microinclusions of zircon (Zr), (B) ilmenite (Ilm), and (C) fluorite (Fl), carbonate (Cb), and presence of overgrown K-feldspar (Kfs).

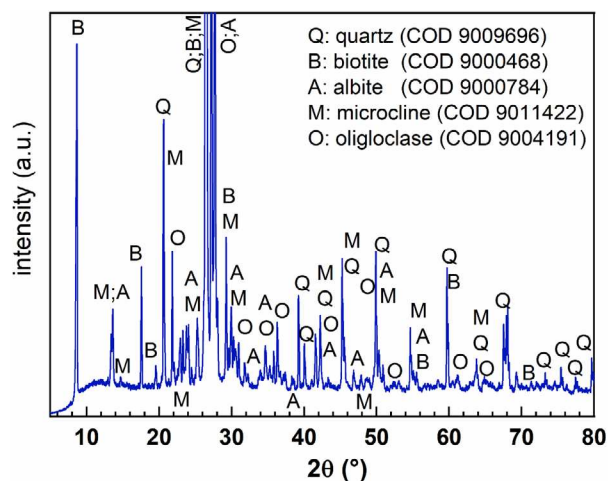


Figure 7. Representative diffractogram of the Rio dos Remédios metarhyolites. The main mineral phases are quartz, microcline, oligoclase, albite, and biotite.

(A), which possibly represent the albite intergrown in the K-feldspar, not identifiable in the petrographic investigation.

Mineral chemistry

Feldspar phenocrysts are mostly pure orthoclase ($\text{Or}_{96.5-98.1}\text{Ab}_{1.6-3.4}\text{An}_{0.1}$), with of formula unit ($\text{Na}_{0.02-0.04}\text{K}_{0.98-1.02}\text{Al}_{0.97-1.02}\text{Si}_3\text{O}_8$), though one sample has a sanidine chemical affinity ($\text{Or}_{69.1}\text{Ab}_{30.9}$) (Fig. 8A). The BaO content varies from 0.05 to 0.25%, whereas K_2O varies from 11.5 to 17% and Na_2O between 0.18 and 3.4% (Table 1).

The white mica, previously interpreted as primary muscovite in the petrography, has relatively high contents of FeO and low contents of MgO with an average formula unit of $\text{K}_{0.85-0.96}\text{Al}_{1.23-1.61}(\text{Si}_{3.20-3.72}\text{Al}_{0.27-0.79}\text{O}_{20})(\text{OH},\text{F})_4$ (Table 2). When classified according to the Guidotti (1987) diagram, most samples plot within the muscovite group field, exhibiting chemical similarities with ferrimuscovite and ferriphengite compositions, whereas one plot fits with pure phengite (Fig. 8B).

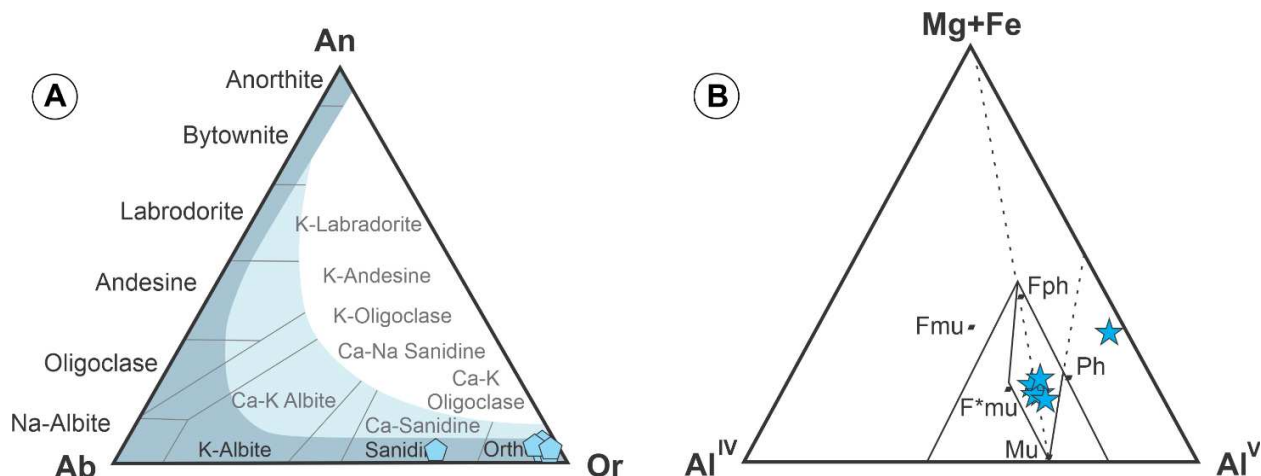
The analyzed biotite flakes (Table 3) can be classified into two groups. In the ternary diagram of Nachit *et al.* (2005), the data reflect differences on the basis of TiO_2 , FeO, MnO, and MgO contents. Group I can be classified as primary biotite, whereas group II crystals fit within neoformed biotite (Fig. 9A).

Group I micas are akin to phlogopite-rich members in the solid solution annite-phlogopite, with X_{Mg} varying between 0.03 and 0.04 and X_{Fe} varying from 0.79 to 0.81. The average formula unit is $(\text{Na}_{0.00-0.01}\text{K}_{0.95-1.00}\text{Ca}_{0.00-0.001})(\text{Al}_{0.24-0.29}\text{Mg}_{0.10-0.11}\text{Fe}_{2.19-2.29})(\text{Al}_{0.24-0.29}\text{Si}_{2.74-2.80}\text{O}_{10})(\text{OH},\text{F})_2$. Considering the relationship of $^{\text{IV}}\text{Al}$ versus $\text{Fe}/(\text{Fe} + \text{Mg})$, group I biotite is mainly characterized by phlogopite and eastonite compositions (Fig. 9B), while members of group II have considerably higher FeO content, coupled with low concentrations of TiO_2 , which is akin to the chamosite end member, also characterized by $\text{Fe}/(\text{Fe} + \text{Mg})$ ratios of around 0.99.

The chlorite classification diagram shows the compositional variation between primary magmatic and chloritized biotite crystals, which reflects differences in iron, magnesium, and aluminum contents. For instance, changes between Mg and Fe indicate a replacement process that resulted in Fe-rich chlorite pseudomorphs (Fig. 9C), whereas the observed changes on Na and K contents represent the losses during chloritization (Wu *et al.* 2019).

DISCUSSION

Blue quartz-bearing rocks are unique within the continental crust, and less is known about its primary aspects in South America, which is only known by small-scale geological maps (*e.g.*, Arcanjo *et al.* 1999, Santos *et al.* 2012, Santos *et al.* 2019), and the uniqueness of each occurrence represents a major gap on their origin. All the studied metavolcanic rocks from the Novo Horizonte Formation exhibit similar chemical and petrographical data. The identified mineral assemblage fits with common acid effusive rocks, reflecting the original magmatic composition, composed of quartz, K-feldspar, plagioclase, biotite, muscovite, fluorite, allanite, rutile, zircon, opaque minerals (mostly magnetite and hematite), and secondary phases,



Mu: muscovite; Ph: phengite; Fph: ferriphengite; Fmu: ferrimuscovite; F*mu: second type of ferrimuscovite.

Figure 8. (A) An-Ab-Or ternary diagram for feldspar classification (Deer *et al.* 1992). (B) Muscovite chemical classification diagram (Guidotti 1987).

Table 1. Representative electron microprobe analyses (in wt.%) of feldspar in the metarhyolite samples.

Mineral	Fds	Fds	Fds	Fds	Fds	Fds	Fds
Sample	P5	P5	P6	P6	P5	P5	P5
Analysis	Q4-Kf1	Q4-Kf2	Qz6-Kf1	Qz6-Kf2	Q3-Kf1	Q3-Kf2	Q3-Kf3
SiO ₂	64.06	64.13	66.00	65.38	64.62	64.09	64.09
Al ₂ O ₃	17.55	17.55	18.72	18.40	18.42	18.42	18.70
FeO	0.25	0.23	0.04	0.06	0.01	0.01	0.06
CaO	0.03	0.01	n.d.	n.d.	n.d.	n.d.	n.d.
Na ₂ O	0.33	0.24	3.41	0.18	0.39	0.39	0.22
K ₂ O	16.98	17.01	11.58	16.95	16.60	16.60	16.90
BaO	0.22	0.05	0.06	0.09	0.06	0.06	0.21
Sum	99.47	99.22	99.81	101.06	100.10	99.55	100.18
Si (apfu)	3.00	3.01	3.00	3.00	2.99	2.98	2.97
Al	0.97	0.97	1.00	1.00	1.01	1.01	1.02
Fe	0.01	0.01	0.00	0.00	0.00	0.00	0.00
Ca	0.00	0.00	0.00	0.00	0.00	0.00	0.00
Na	0.03	0.02	0.30	0.02	0.04	0.04	0.02
K	1.02	1.02	0.67	0.99	0.98	0.99	1.00
X	1.06	1.05	0.98	1.01	1.02	1.02	1.03
Z	3.97	3.98	4.01	3.99	4.00	4.00	4.00
Or	97.00	97.90	69.10	98.40	96.60	96.60	98.10
Ab	2.90	2.10	30.90	1.60	3.40	3.40	1.90
An	0.10	0.00	0.00	0.00	0.00	0.00	0.00

apfu: atoms per formula unit. The structural formula was calculated using eight oxygens; n.d.: not determined.

including carbonate, sericite, and phengite. However, evidence for later ductile deformation is present, interpreted as the result of tectonic inventions of the Brasiliano Orogeny (*e.g.*, Brito Neves *et al.* 2014).

The samples show mineralogy and mineral chemistry typical of strongly peraluminous and alkaline magmas, common in anorogenic settings (Abdel-Rahman 1994), and typical of blue quartz host rocks (Zolensky *et al.* 1988). The observed igneous paragenesis fits with the previous whole-rock geochemical interpretations of the Rio dos Remédios metavolcanic rocks association (*e.g.*, Teixeira 2005, Guimarães *et al.*

2008, Santos *et al.* 2019). Such an inference is strongly based on the observed equilibrium paragenesis of the muscovite-biotite pair, a trustful petrological indicator of magma composition (Abdel-Rahman 1994).

Despite the primary mineralogy present in those samples, one must consider the role of metasomatic and deformational processes of variable crustal regimes, as attested by the extremely fractured, recrystallized, and altered crystals, as well as the widespread evidence for the formation of sericite and carbonate veins. We interpreted these events as coeval to the regional ductile deformation, possibly triggered by the

Table 2. Representative electron microprobe analyses (in wt.%) of muscovite in the studied metarhyolite samples.

Mineral	Ms	Ms	Ms	Ms	Ms	Ms
Sample	P5	P5	P5	P5	P5	P5
Analysis	Fd2-6	Fd2-7	Fd2-8	Fd2-9	Fd2-10	Fd2-11
Na ₂ O	1.34	0.15	0.11	0.08	0.18	0.15
SiO ₂	52.71	47.49	46.72	45.72	45.73	46.76
MgO	0.17	0.49	0.53	0.47	0.42	0.48
Al ₂ O ₃	18.02	29.49	28.37	28.86	28.48	28.94
K ₂ O	10.66	10.18	10.24	10.36	10.29	9.71
CaO	0.24	0.00	0.02	0.02	0.00	0.01
TiO ₂	0.00	0.41	0.38	0.30	0.43	0.23
Cr ₂ O ₃	n.d.	n.d.	n.d.	n.d.	n.d.	n.d.
MnO	0.17	0.07	0.01	0.06	0.05	0.03
FeO	11.30	7.52	7.52	7.92	8.49	7.38
Sum	94.61	95.80	93.90	93.79	94.07	93.69
Si (apfu)	3.72	3.23	3.25	3.20	3.20	3.24
Ti	0.00	0.02	0.01	0.01	0.02	0.01
Al ^{IV}	0.27	0.76	0.74	0.79	0.79	0.75
Al ^{VI}	1.23	1.60	1.58	1.58	1.55	1.61
Cr	0.00	0.00	0.00	0.00	0.00	0.00
Fe	0.66	0.42	0.43	0.46	0.49	0.42
Mg	0.17	0.04	0.05	0.04	0.04	0.04
Mn	0.01	0.00	0.00	0.00	0.00	0.00
Ca	0.01	0.00	0.00	0.00	0.00	0.00
Na	0.18	0.01	0.01	0.01	0.02	0.02
K	0.92	0.88	0.90	0.92	0.91	0.86

apfu: atoms per formula unit; n.d.: not determined.

Table 3. Representative electron microprobe analyses (in wt.%) of biotite in the studied metarhyolite samples.

Mineral	Bt	Bt	Bts	Bt	Bt	Bt
Sample	P5	P5	P5	P5	P5	P5
Analysis	Qz-Bt1	Qz-Bt2	Qz-Bt3	Fd2-3	Fd2-4	Fd2-6
Na ₂ O	0.11	0.04	0.10	0.07	0.08	0.11
SiO ₂	35.54	33.30	33.41	25.53	25.53	27.17
MgO	0.90	0.94	0.90	0.34	0.37	0.27
Al ₂ O ₃	15.47	15.23	16.12	14.60	14.78	13.98
K ₂ O	9.52	9.52	9.60	0.20	0.26	0.43
CaO	0.02	0.00	0.02	0.54	0.55	0.70
TiO ₂	2.73	2.75	2.83	0.03	0.03	0.03
Cr ₂ O ₃	0.02	n.d.	0.00	0.00	0.00	n.d.
MnO	0.18	0.17	0.16	0.05	0.50	0.98
FeO	34.75	33.02	32.06	44.46	44.12	43.24
Sum	99.24	94.97	95.20	86.27	86.43	86.91
Si (apfu)	2.80	2.75	2.74	2.42	2.43	2.54
Ti	0.16	0.17	0.17	0.00	0.00	0.00
Al ^{IV}	1.19	1.24	1.25	1.57	1.56	1.45
Al ^{VI}	0.24	0.24	0.29	0.05	0.08	0.08
Cr	0.00	0.00	0.00	0.00	0.00	0.00
Fe	2.29	2.28	2.19	3.53	3.48	3.38
Mg	0.10	0.11	0.11	0.04	0.05	0.03
Mn	0.01	0.01	0.01	0.04	0.04	0.07
Ca	0.00	0.00	0.00	0.05	0.05	0.07
Na	0.01	0.00	0.01	0.01	0.01	0.01
K	0.95	1.00	1.00	0.02	0.03	0.05

apfu: atoms per formula unit; n.d.: not determined.

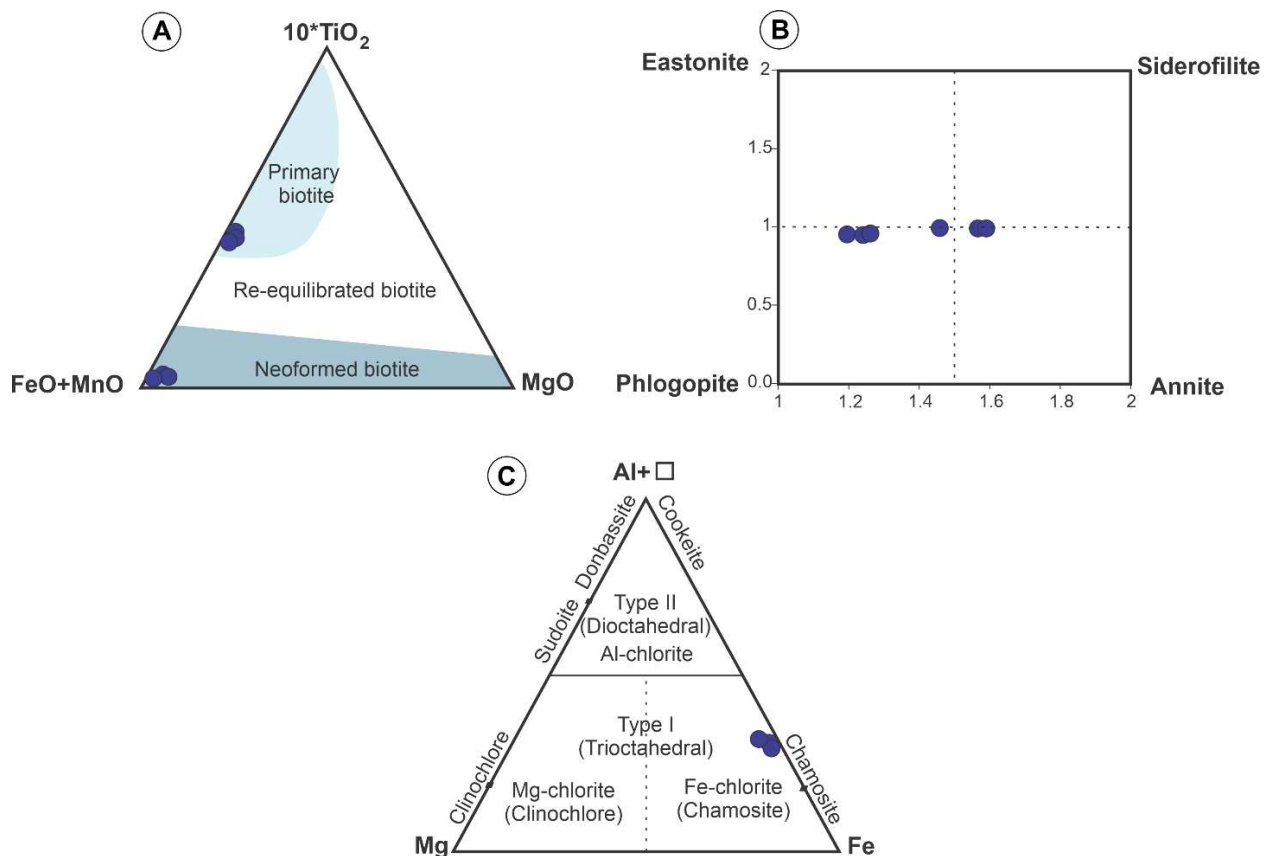


Figure 9. (A) Fe# vs. Al^{IV} for biotite classification (Deer 1992). (B) TiO_2 - FeO_1 - MgO ternary diagram for biotite classification (Nachit *et al.* 2005); (C) $(\text{Al}+\square)$ -Mg-F compositional classification diagram of chlorite (Zane and Weiss 1998). \square represents structure vacancies. Black dots represent end members.

migration of fluids in an intercrystalline form, destabilizing lesser stable phases (Santos *et al.* 2019), as evidenced by the described microstructures.

Rounded and embayed quartz phenocrysts, usually referred to as “quartz eyes,” occur in association with processes correlated to crystallization at high temperature, crystallization in a magmatic-hydrothermal system, disaggregation, and recrystallization of early quartz-rich bodies (Betsi and Lentz 2010).

However, during deformation, conditions of reduction of elastic distortional energy, which occurs by the concentration of dislocation into walls, are driven to subgrain rotation. Thus, the crystal reaches extinction at slightly different angles, proving a mottled appearance, and there is the formation of small new grains, which are consistent with the deformation of preexisting phenocrysts (Guillope and Poirier 1979).

The presence of K-feldspar megacrysts is associated with the relatively small amount of calcic plagioclase and mafic components in metaluminous and peraluminous granitoid systems, suggesting that a large amount of liquid is still available when K-feldspar begins to crystallize (Vernon 1986). According to Winkler and Schultes (1982), about 60–70 wt.% of the liquid remains when K-feldspar starts to precipitate. Early crystallization of small amounts of mafic minerals, plagioclase, and quartz might take place; in this case, the abundance of silica in the magma provides a high probability for the formation of large, ovoid to lenticular quartz phenocrysts.

When K-feldspar grows rapidly, there is plenty of space for them to expand, move, or incorporate other small phenocrysts.

Thus, early crystallization of K-feldspar does not constitute the only explanation to form the megacrysts, since their formation is supposed to be part of a solid state, since the only requirement is enough to melt (30–40% at least; Vernon 1986). On the contrary, the groundmass tends to deform relative to the phenocrysts, due to its fine grain size and composition (Vernon 1986). Those characteristics are consistent with the deformation of the matrix containing preexisting large grains (Bradley 1957).

The hydrothermal processes are well marked on biotite crystals, since their cleavage planes enable the percolation of hydrothermal fluids. For instance, its Ti content is commonly controlled thermally; therefore, re-equilibrated and neoformed biotite lamellae might represent low-temperature hydrothermal reactions, which are characterized by low contents of Ti, as characterized by the group II biotites of the Novo Horizonte metarhyolite (Zhang *et al.* 2016).

The formation of chlorite might also be interpreted as a fluid-rock reaction process, which is generally controlled by the reaction kinetics (Zhang *et al.* 2007). The chloritization of Novo Horizonte metarhyolites occurs when biotite is partially metasomatized, leading to chlorite growth. In addition, the chemical composition of chlorite crystals indicates that the fluids are rich in Fe or that they might have been able to extract Fe components of the host rock during metasomatic events. Thus, the formation of chlorite could be associated with dissolution-precipitation mechanisms, manifested by hydrothermal fluid metasomatized biotite (Zhang *et al.* 2006, Wu *et al.* 2019).

The abundance of albite revealed by the XRD analysis could also be explained by the presence of late metasomatic fluids, forming intergrowths of albite in K-feldspar and granophyric texture of quartz in K-feldspar. According to Barker and Burmester (1970) and Cox *et al.* (1979), granophyric textures usually result from a silicate melt at the eutectic point, or in the presence of a water-rich phase, when the magma is significantly undercooled. Allanite could also have been introduced into the system by rare earth element-bearing fluids (Gros *et al.* 2020).

The combination of field relationships, mineral assemblage, and chemistry of these rocks is in accordance with an intraplate environment, associated with the continental rift of the Chapada Diamantina. Rhyolite origin in intraplate continental settings is strongly related to the interaction of primary mafic magma with the surrounding crust, at crustal depths (Halder *et al.* 2021). The partial melting of an underplated mantle, with the intrusion of crustal material, triggering hydrothermal reactions, is a good model to explain the origin of the Rio dos Remédios metarhyolites.

CONCLUSION

The metarhyolites from the Novo Horizonte Formation show a characteristic mineral assemblage formed by quartz, K-feldspar, biotite, muscovite, zircon, ilmenite, and rutile. High silica and peraluminous metarhyolites show transitional magmatic affinities and intraplate crustal-derived A-type signatures.

The mineral assemblage exhibits features of deformational and associated hydrothermal alteration. The hydrothermal processes are marked by the complete or partial replacement of some mineral phases, forming secondary assemblages,

mainly represented by chlorite, sericite, phengite, and carbonate. The compositional differences of biotite types and the presence of allanite are also great evidence of fluid action.

Deformational effect is well marked by the abutment of groundmass foliation against phenocrysts, rather than deflection around them. Due to the presence of megacrysts, the fine-grained, polymineralic aggregates of the matrix have the tendency to undergo deformation (Vernon 1986).

Despite the alteration on these rocks, the east portion of the body was more affected, forming garnet and kyanite phases (Santos *et al.* 2019). Therefore, the Paramirim portion would be a better representative of the primary features of the Rio dos Remédios. Nevertheless, the characterization of these processes is challenging due to the Brasiliano overprinting.

ACKNOWLEDGMENTS

This work is part of the first author's MSc dissertation, which has been supported by grants provided by the Universidade Federal de Pernambuco and the Instituto Nacional de Ciência e Tecnologia (INCT) para Estudos Tectônicos. We are indebted to the Conselho Nacional de Desenvolvimento Científico e Tecnológico (CNPq) of Brazil for the first author's scholarship. We also thank the Microscopy and Microanalysis Laboratory of the Universidade Federal de Ouro Preto, a member of the Fundação de Amparo à Pesquisa do Estado de Minas Gerais (FAPEMIG). L. Montefalco and G. Queiroga are fellows of the Brazilian Research Council (CNPq) and acknowledge the support given. We would like to express our gratitude to Prof. Pedro Luiz Guzzo (UFPE) for the x-ray analysis performed at the Laboratório de Tecnologia Mineral (LTM) as well as his contributions on the manuscript.

ARTICLE INFORMATION

Manuscript ID: 20220034. Received on: 26 APR 2022. Approved on: 25 OCT 2022.

How to cite this article: Silva D.C., Montefalco L., Queiroga G., Santos G.L., Tedeschi M. 2023. Multi-method characterization of rare blue quartz-bearing metavolcanic rocks of the Rio dos Remédios Group, Paramirim Aulacogen, NE Brazil. *Brazilian Journal of Geology*, 53(1): e20220034. <https://doi.org/10.1590/2317-4889202320220034>

D.C.S.: Conceptualization, data curation, formal analysis, investigation, methodology, resources, software, supervision, validation, visualization, writing — original draft, and writing — review & editing. L.C.M.L.S.: Conceptualization, data curation, funding acquisition, investigation, methodology, project administration, resources, supervision, validation, visualization, and writing — review & editing. G.N.Q. and M.T.: Conceptualization, data curation, formal analysis, funding acquisition, investigation, methodology, resources, software, validation, and writing — review & editing. G.L.S.: Conceptualization, investigation, resources, validation, visualization, writing — original draft, and writing — review & editing.

Competing interest: the authors declare no competing interests.

REFERENCES

- Abdel-Rahman A.F.M. 1994. Nature of biotites from alkaline, calc-alkaline, and peraluminous magmas. *Journal of Petrology*, 35(2):525-541. <https://doi.org/10.1093/petrology/35.2.525>
- Alkmim F.F., Brito Neves B.B., Alves J.A.C. 1993. Arcabouço tectônico do Cráton do São Francisco – uma revisão. In: Dominguez J.M., Misi A. (eds.). O cráton do São Francisco. *Reunião preparatória do II Simpósio sobre o cráton do São Francisco*. Salvador: SBG/Núcleo BA/SE/SGM/CNPq. p. 45-62.
- Alkmim F.F., Pedrosa-Soares A.C., Noce C.M., Cruz S.C.P. 2007. Sobre a evolução tectônica do Orógeno Araçuaí-Congo Ocidental. *Geonomos*, 15(1):25-43. <https://doi.org/10.18285/geonomos.v15i1.105>
- Almeida F.F.M. 1977. O Cráton do São Francisco. *Revista Brasileira de Geociências*, 7(4):349-364.
- Arcanjo J.B.A., Varela P.H.L., Martins A.A.M., Loureiro H.S.C., Neves J.P. (Eds.). 1999. *Projeto Vale do Paramirim: Estado da Bahia. Programa Levantamentos Geológicos Básicos do Brasil - PLGB. Convênio CBPM/CPRM. Escala 1:200.000. Relatório interno*. Salvador: CPRM Bahia.
- Babinski M., Brito Neves B.B., Machado N., Noce C.M., Uhlein A., Vanschmus W.R. 1994. Problemas da metodologia U/Pb em zircões de vulcânicas continentais: caso do Grupo Rio dos Remédios, Supergrupo Espinhaço, no Estado da Bahia. In: 42° Congresso Brasileiro de Geologia, 42., 1994. *Anais... Sociedade Brasileira de Geologia, Balneário Camboriú, 2:409-410*.

- Barbosa J.S.F. 2012. *Geologia da Bahia: pesquisa e atualização*. Salvador: CBPM, p. 33-85. 2 v. (Série de publicações especiais; 13).
- Barbosa J.S.F., Sabaté P. 2003. Colagem Paleoproterozóica de Placas Arqueanas do Cráton do São Francisco na Bahia. *Revista Brasileira de Geociências*, **33**(1):714.
- Barker D.S., Burmester R.F. 1970. Leaching of quartz from precambrian hypabyssal rhyolite porphyry, Llano County, Texas. *Contributions to Mineralogy and Petrology*, **28**(1):1-8. <https://doi.org/10.1007/BF00389222>
- Betsi T.B., Lentz D.R. 2010. The nature of "quartz eyes" hosted by dykes associated with Au-Bi-As-Cu, Mo-Cu, and base-metal-Au-Ag mineral occurrences in the mountain freegold region (Dawson Range), Yukon, Canada. *Journal of Geosciences*, **55**(4):347-368. <https://doi.org/10.3190/jgeosci.082>
- Bradley J. 1957. Geology of the West Coast Range, part III: Porphyroid metassomatism. *Papers and Proceedings of the Royal Society of Tasmania*, **91**:163-190.
- Brito Neves B.B., Fuck R.A., Pimentel M.M. 2014. A colagem Brasileira na América do Sul: uma revisão. *Brazilian Journal of Geology*, **44**(3):493-518. <https://doi.org/10.5327/Z2317-4889201400030010>
- Carlin A.C., Zanardo A., Navarro G.R.B. 2018. Caracterização petrográfica das rochas encaixantes da mineralização aurífera do Depósito Lavra Velha – região de Ibitiara, borda oeste da Chapada Diamantina, Bahia. *Geociências Unesp*, **37**(2):253-265. <https://doi.org/10.5016/geociencias.v37i2.12113>
- Cavalcanti J.C.C., Moreira M.D., Oliveira W.D., Siqueira A.P., Silva B.C.E., Cunha J.C., Monteiro M.D., Oliveira N.D., Araújo N.B., Fróes R.J.B., Souza S.L. 1980. Projeto prospecção de cassiterita na Chapada Diamantina-BA. *Companhia Baiana de Produção Mineral*, 123 p.
- Caxito F.A., Santos L.C.M.L., Ganade de Araújo C.E., Bendaoud A., Fettous E.-H., Bouyo Houketchang N. 2020. Toward an integrated model of geological Evolution for NE Brazil-NW Africa: The Borborema Province and its connections to the Trans-Saharan (Benino-Nigerian and Tuareg shields) and Central African orogens. *Brazilian Journal of Geology*, **50**(2):1-38. <https://doi.org/10.1590/2317-4889202020190122>
- Cox K.G., Bell J.D., Pankhurst R.J. 1979. *The Interpretation of Igneous Rocks*. London: George Allen and Unwin, 450 p.
- Cruz S.C.P., Alkmim F.F. 2017. The Paramirim Aulacogen. In: Heilbron, M., Cordani, U.G., Alkmim F.F. (Eds.). *São Francisco Craton, Eastern Brazil*. Springer, **1**:97-115. <https://doi.org/10.1007/978-3-319-01715-0>
- Cruz S.C.P., Dias V.M., Alkmim F.F. 2007. A interação tectônica embasamento/coertura em aulacógenos invertidos: um exemplo da Chapada Diamantina Ocidental. *Revista Brasileira de Geociências*, **37**(4):111-127.
- Danderfer Filho A., Dardenne M.A. 2002. Tectonoestratigrafia da bacia Espinhaço na porção centro-norte do Cráton do São Francisco: registro de uma evolução poliistórica descontínua. *Revista Brasileira de Geociências*, **32**(4):449-460.
- Danderfer Filho A., Lana C.C., Nalini Júnior H.A., Costa A.F.O. 2014. Constraints on the Statherian evolution of the intraplate rifting in a Paleoproterozoic paleocontinent: New stratigraphic and geochronology record from the eastern São Francisco craton. *Gondwana Research*, **28**(2):668-688. <https://doi.org/10.1016/j.gr.2014.06.012>
- Deer W.A., Howie R.A., Zussman J. 1992. *An introduction to the rock-forming minerals*. Harlow: Longman Scientific and Technical.
- Dörfler H.D. 2002. *Grenzflächen und colloid-disperse Systeme*. Berlin: Springer, 989 p.
- Etheridge A., Vernon R.H. 1981. A deformed polymictic conglomerate - the influence of grain size and composition on the mechanism and rate of deformation. *Tectonophysics*, **79**(3-4):237-254. [https://doi.org/10.1016/0040-1951\(81\)90115-3](https://doi.org/10.1016/0040-1951(81)90115-3)
- Gao P., Garcia-Arias M., Chen Y.X., Zhao Z.F. 2020. Origin of peraluminous A-type granites from appropriate sources at moderate to low pressures and high temperatures. *Lithos*, **352-353**:105287. <https://doi.org/10.1016/j.lithos.2019.105287>
- Gros K., Slaby E., Jokubauskas P., Sláma J., Kozub-Budzyn. 2020. Allanite geochemical response to hydrothermal alteration by alkaline, low-temperature fluids. *Minerals*, **10**(5):392-422. <https://doi.org/10.3390/min10050392>
- Guadagnin F., Chemale Jr. F. 2015. Detrital zircon record of the Paleoproterozoic to Mesoproterozoic cratonic basins in the São Francisco Craton. *Journal of South American Earth Sciences*, **60**:104-116. <https://doi.org/10.1016/j.jsames.2015.02.007>
- Guidotti C.V. 1987. Compositional variations of muscovite as a function of metamorphic grade and assemblage in metapelites from N.W. Maine. *Contributions to Mineralogy and Petrology*, **41**:33-42.
- Guillope M., Poirier J.P. 1979. Dynamic recrystallization during creep of single-crystalline halite: an experimental study. *Journal of Geophysical Research*, **84**(B10):5557-5567. <https://doi.org/10.1029/JB084iB10p05557>
- Guimarães J.T., Alkmim F.F., Cruz S.C.P. 2012. Supergrupos Espinhaço e São Francisco. In: Barbosa J.S.F., Mascarenhas J., Domingues J.M.L., Correa-Gomes L.C. *Geologia da Bahia: pesquisa e atualização de dados*. Salvador: CBPM.
- Guimarães J.T., Martins A.A.M., Andrade Filho E.L., Loureiro H.S.C., Arcanjo J.B.A., Abram M.B., Silva M.G., Bento R.V. 2008. *Projeto Ibitiara-Rio de Contas*. Série Arquivos Abertos; 31. Salvador: CPRM-Bahia, 70 p.
- Guimarães J.T., Martins A.A.M., Loureiro H.S.C., Arcanjo J.B.A., Neves J.P., Abram M.B., Silva M.G., Melo R.C., Bento R.V. 2005. *Projeto Ibitiara - Rio de Contas*. Salvador: CPRM/CBPM, Programa Recursos Minerais do Brasil, 182 p.
- Halder M., Paul D., Sensarma S. 2021. Rhyolites in continental mafic large igneous provinces: petrology, geochemistry and petrogenesis. *Geoscience Frontiers*, **12**(1):53-80. <https://doi.org/10.1016/j.gsf.2020.06.011>
- Heilbron M., Cordani U.G., Alkmim F.F. 2017. *São Francisco Craton, eastern Brazil: tectonic genealogy of a miniature continent*. New York: Regional Geology Reviews, Springer Berlin Heidelberg, 331 p. <https://doi.org/10.1007/978-3-319-01715-0>
- Iddings J.P. 1904. Quartz-feldspar-porphyry (graniphyroliparose-alakose) from Llano, Texas. *Journal of Geology*, **12**(3):225-231. <https://doi.org/10.1086/621145>
- Loureiro H.S.C., Guimarães J.T., Martins A.A.M., Andrade E.L., Arcanjo J.B.A., Neve J.P., Abram M.B., Silva M.G., Melo R.C. 2008. *Projeto Barra-Oliveira dos Brejinhos, Estado da Bahia*. Salvador: Companhia Brasileira de Pesquisa Mineral e CPRM, 156 p.
- Medeiros K.O.P. 2013. *Estratigrafia de Sequências do Supergrupo Espinhaço na Região Entre Macaúbas e Canatiba - Bahia*. MS Dissertation, Instituto de Geociências, Universidade Federal da Bahia, Salvador, 102 p.
- Nachit H., Ibbi A., Abia E.H., Ohoud M.B. 2005. Discrimination between Primary Magmatic Biotites, Reequilibrated Biotites and Neoformed Biotites. *Comptes Rendus Geoscience*, **337**(16):1415-1420. <https://doi.org/10.1016/j.crte.2005.09.002>
- Pantia A.I., Filuță A., Lórinç S. 2019. Blue quartz around the globe. *Muzeul Olteniei Craiova. Oltenia. Studii și comunicări. Științele Naturii*, **35**(2).
- Rosa M.L.S. 1999. *Geologia, geocronologia, mineralogia, litogeoquímica e petrologia do Batólito Monzo-Sientífico Guanambi-Urandi (SW-Bahia)*. PhD Thesis, Universidade Federal da Bahia, Salvador, 186 p.
- Santana A.V.A. 2016. *Análise estratigráfica em alta resolução: exemplo em rampa carbonática dominada por microbialitos da Formação Salitre, Bacia do Irecê, Bahia*. PhD Thesis, Universidade de Brasília, Brasília, 183 p.
- Santos J.M.A., Machado A., Lenz C., Liz L.C.C., Costa I.A.A. 2019. Geologia, petrografia e geoquímica das rochas metavulcânicas ácidas da Estrada Real, Rio de Contas (BA). *Pesquisas em Geociências*, **46**(2):e699. <https://doi.org/10.22456/1807-9806.95462>
- Santos L.C.M.L., Santos E.J., Dantas E.L., Lima H.M. 2012. Análise estrutural e metamórfica da região de Sucuru (Paraíba): implicações sobre a evolução do Terreno Alto Moxotó, Província Borborema. *Geologia USP. Série Científica*, **12**(3):5-20. <https://doi.org/10.5327/Z1519-874X2012000300001>
- Schobbenhaus C. 1996. As tafrogêneses superpostas Espinhaço e Santo Onofre, Estado da Bahia: Revisão e novas propostas. *Revista Brasileira de Geociências*, **26**(4):265-276.

- Schobbenhaus C., Hoppe A., Baumann A. 1994. Idade U/Pb do vulcanismo Rio dos Remédios, Chapada Diamantina, Bahia. In: Congresso Brasileiro de Geologia, Balneário Camboriú, 38., 1994. *Boletim de Resumos Expandidos*, 2:397-398.
- Schobbenhaus C., Kaul P.F.T. 1971. Contribuição à estratigrafia da Chapada Diamantina Bahia Central. *Mineração e Metalurgia*, 53:116-120.
- Seifert W., Rhede D., Thomas R., Förster H. J., Lucassen F., Dulski P., Wirth R. 2011. Distinctive properties of rock-forming blue quartz: inferences from a multi-analytical study of submicron mineral inclusions. *Mineralogical Magazine*, 75(4):2519-2534. <https://doi.org/10.1180/minmag.2011.075.4.2519>
- Silva F.F., Oliveira D.C., Antonio P.Y.J., D'agrella Filho M.S., Lamarão C.N. 2016. Bimodal magmatism of the Tucumã area, Carajás province: U-Pb geochronology, classification and processes. *Journal of South American Earth Sciences*, 72:95-114. <https://doi.org/10.1016/j.jsames.2016.07.016>
- Teixeira L.R. 2005. *Projeto Ibitiara-Rio de Contas: relatório temático de litogeoquímica*. Programa Levantamentos Geológicos Básicos do Brasil. Relatório interno. Salvador: CPRM, 33 p.
- Vernon R.H. 1986. Evaluation of the 'quartz-eye' hypothesis. *Economic Geology*, 81(6):1520-1527. <https://doi.org/10.2113/gsecongeo.81.6.1520>
- Vernon R.H. 1990. K-feldspar augen in felsic gneisses and mylonites—deformed phenocrysts or porphyroblasts? *Geologiska Föreningen i Stockholm Förhandlingar*, 112(2):157-167. <https://doi.org/10.1080/11035899009453175>
- Williams M.L., Burr J.L. 1994. Preservation of quartz phenocrysts and kinematic indicators in metamorphosed and deformed Proterozoic rhyolites, southwestern North America. *Journal of Structural Geology*, 16(2):203-221.
- Winkler H.G.F., Schultes H. 1982. On the problem of alkali feldspar phenocrysts in granitic rocks. *Neues Jahrbuch für Mineralogy*, 12:558-564.
- Wright T.L., Stewart D.B. 1968. X-ray and optical study of alkali feldspar: I. Determination of composition and structural state from refined unit-cell parameters and 2V. *American Mineralogist*, 53(1-2):38-87.
- Wu D.J.P., Fei Xia G.H., Jing L. 2019. The mineral chemistry of chlorites and its relationship with uranium mineralization from Huangsha uranium mining area in the middle Nanling Range, SE China. *Minerals*, 9(3):199. <https://doi.org/10.3390/min9030199>
- Zane A., Weiss Z. 1998. A procedure for classifying rock-forming chlorites based on microprobe data. *Rendiconti Lincei*, 9:51-56. <https://doi.org/10.1007/BF02904455>
- Zhang H.F., Zhang L., Harris N., Jin L.L., Yuan H.L. 2006. U-Pb zircon ages, geochemical and isotopic compositions of granitoids in Songpan-Garze fold belt, eastern Tibetan Plateau: constraints on petrogenesis and tectonic evolution of the basement. *Contributions to Mineralogy and Petrology*, 152(1):75-88. <https://doi.org/10.1007/s00410-006-0095-2>
- Zhang W., Lentz D.R., Thorne K.G., McFarlane C. 2016. Geochemical characteristics of biotite from felsic intrusive rocks around the Sisson Brook W-Mo-Cu deposit, west-central New Brunswick: an indicator of halogen and oxygen fugacity of magmatic systems. *Ore Geology Review*, 77:82-96. <https://doi.org/10.1016/j.oregeorev.2016.02.004>
- Zhang Z.S., Hua R.M., Ji J.F., Zhang Y.C., Guo G.L., Yin Z.P. 2007. Characteristics and formation conditions of chlorite in N°. 201 and N°. 361 uranium deposits. *Acta Mineralogy*, 27:161-172.
- Zolensky M.E., Sylvester P.J., Paces J.B. 1988. Origin and significance of blue coloration in quartz from Llano rhyolite (llanite), north-central Llano County, Texas. *American Mineralogist*, 73:313-332.